

High peak-power picosecond pulse generation at 1.26 μm using a quantum-dot-based external-cavity mode-locked laser and tapered optical amplifier

Y. Ding,^{1,*} R. Aviles-Espinosa,² M. A. Cataluna,¹ D. Nikitichev,¹ M. Ruiz,³ M. Tran,³ Y. Robert,³ A. Kapsalis,⁵ H. Simos,⁵ C. Mesaritakis,⁵ T. Xu,⁴ P. Bardella,⁴ M. Rossetti,⁴ I. Krestnikov,⁶ D. Livshits,⁶ Ivo Montrosset,⁴ D. Syvridis,⁵ M. Krakowski,³ P. Loza-Alvarez,² and E. Rafailov¹

¹*School of Engineering, Physics and Mathematics, University of Dundee, Dundee DD1 4HN, UK*

²*ICFO – The Institute of Photonic Sciences, Mediterranean Technology Park, Av. Carl Friedrich Gauss, 3, 08860 Castelldefels (Barcelona), Spain*

³*III-V Lab, 1 Av. Augustin Fresnel, Campus de Polytechnique, 91767 Palaiseau, France*

⁴*Dipartimento di Elettronica e Telecomunicazioni, Politecnico di Torino, I-10129 Turin, Italy*

⁵*National and Kapodistrian University of Athens, Panepistimiopolis, Ilissia, Athens 15784, Greece*

⁶*Innolume GmbH, Konrad-Adenauer-Allee 11, 44263 Dortmund, Germany*

[*y.ding@dundee.ac.uk](mailto:y.ding@dundee.ac.uk)

Abstract: In this paper, we present the generation of high peak-power picosecond optical pulses in the 1.26 μm spectral band from a repetition-rate-tunable quantum-dot external-cavity passively mode-locked laser (QD-ECMLL), amplified by a tapered quantum-dot semiconductor optical amplifier (QD-SOA). The laser emission wavelength was controlled through a chirped volume Bragg grating which was used as an external cavity output coupler. An average power of 208.2 mW, pulse energy of 321 pJ, and peak power of 30.3 W were achieved. Preliminary nonlinear imaging investigations indicate that this system is promising as a high peak-power pulsed light source for nonlinear bio-imaging applications across the 1.0 μm - 1.3 μm spectral range.

©2012 Optical Society of America

OCIS codes: (230.5590) Quantum-well, -wire and -dot devices; (140.4050) Mode-locked lasers; (250.5980) Semiconductor optical amplifiers; (180.4315) Nonlinear microscopy.

References and links

1. W. Denk, J. H. Strickler, and W. W. Webb, "2-Photon Laser Scanning Fluorescence Microscopy," *Science* **248**, 73-76 (1990).
2. D. Yelin, D. Oron, E. Korkotian, M. Segal, and Y. Silberberg, "Third-harmonic microscopy with a titanium-sapphire laser," *Appl. Phys. B-Lasers Opt.* **74**, S97-S101 (2002).
3. L. Moreaux, O. Sandre, M. Blanchard-Desce, and J. Mertz, "Membrane imaging by simultaneous second-harmonic generation and two-photon microscopy," *Opt. Lett.* **25**, 320-322 (2000).
4. R. Aviles-Espinosa, G. Filippidis, C. Hamilton, G. Malcolm, K. J. Weingarten, T. Sudmeyer, Y. Barbarin, U. Keller, S. Santos, D. Artigas, and P. Loza-Alvarez, "Compact ultrafast semiconductor disk laser: targeting GFP based nonlinear applications in living organisms," *Biomed. Opt. Express* **2**, 739-747 (2011).
5. Y. Li, M. Breivik, C. Y. Feng, B. O. Fimland, and L. F. Lester, "A Low Repetition Rate All-Active Monolithic Passively Mode-Locked Quantum-Dot Laser," *IEEE Photonics Technol. Lett.* **23**, 1019-1021 (2011).
6. H. Kano and H. Hamaguchi, "In-vivo multi-nonlinear optical imaging of a living cell using a supercontinuum light source generated from a photonic crystal fiber," *Opt. Express* **14**, 2798-2804 (2006).
7. S. Tang, T. B. Krasieva, Z. Chen, G. Tempea, and B. J. Tromberg, "Effect of pulse duration on two-photon excited fluorescence and second harmonic generation in nonlinear optical microscopy," *J. Biomed. Opt.* **11**, 020501 (2006).
8. S. M. Zhuo, J. X. Chen, S. S. Xie, L. Q. Zheng, and Z. B. Hong, "Nonlinear optical microscopy for visualizing dermal structural assembly in normal and pathological human dermis," *Laser Phys. Lett.* **6**, 764-767 (2009).
9. H. Yokoyama, A. Sato, H. C. Guo, K. Sato, M. Murc, and H. Tsubokawa, "Nonlinear-microscopy optical-pulse sources based on mode-locked semiconductor lasers," *Opt. Express* **16**, 17752-17758 (2008).

10. M. Kuramoto, N. Kitajima, H. C. Guo, Y. Furushima, M. Ikeda, and H. Yokoyama, "Two-photon fluorescence bioimaging with an all-semiconductor laser picosecond pulse source," *Opt. Lett.* **32**, 2726-2728 (2007).
 11. K. Taira, T. Hashimoto, and H. Yokoyama, "Two-photon fluorescence imaging with a pulse source based on a 980-nm gain-switched laser diode," *Opt. Express* **15**, 2454-2458 (2007).
 12. D. Kobat, M. E. Durst, N. Nishimura, A. W. Wong, C. B. Schaffer, and C. Xu, "Deep tissue multiphoton microscopy using longer wavelength excitation," *Opt. Express* **17**, 13354-13364 (2009).
 13. I. H. Chen, S. W. Chu, C. K. Sun, P. C. Cheng, and B. L. Lin, "Wavelength dependent damage in biological multi-photon confocal microscopy: A micro-spectroscopic comparison between femtosecond Ti : sapphire and Cr : forsterite laser sources," *Opt. Quantum Electron.* **34**, 1251-1266 (2002).
 14. M. C. Chan, T. M. Liu, S. P. Tai, and C. K. Sun, "Compact fiber-delivered Cr : forsterite laser for nonlinear light microscopy," *J. Biomed. Opt.* **10**, 054006 (2005).
 15. W. J. Lee, C. F. Lee, S. Y. Chen, Y. S. Chen, and C. K. Sun, "Virtual biopsy of rat tympanic membrane using higher harmonic generation microscopy," *J. Biomed. Opt.* **15**, 046012 (2010).
 16. E. U. Rafailov, M. A. Cataluna, and W. Sibbett, "Mode-locked quantum-dot lasers," *Nat. Photonics* **1**, 395-401 (2007).
 17. X. D. Huang, A. Stintz, H. Li, L. F. Lester, J. Cheng, and K. J. Malloy, "Passive mode-locking in 1.3 μm two-section InAs quantum dot lasers," *Appl. Phys. Lett.* **78**, 2825-2827 (2001).
 18. E. U. Rafailov, M. A. Cataluna, W. Sibbett, N. D. Il'inskaya, Y. M. Zadiranov, A. E. Zhukov, V. M. Ustinov, D. A. Livshits, A. R. Kovsh, and N. N. Ledentsov, "High-power picosecond and femtosecond pulse generation from a two-section mode-locked quantum-dot laser," *Appl. Phys. Lett.* **87**, 081107 (2005).
 19. M. G. Thompson, A. R. Rae, X. Mo, R. V. Penty, and I. H. White, "InGaAs Quantum-Dot Mode-Locked Laser Diodes," *IEEE J. Sel. Top. Quantum Electron.* **15**, 661-672 (2009).
 20. M. A. Cataluna, Y. Ding, D. I. Nikitichev, K. A. Fedorova, and E. U. Rafailov, "High-Power Versatile Picosecond Pulse Generation from Mode-Locked Quantum-Dot Laser Diodes " *IEEE J. Sel. Top. Quantum Electron.* **17**, 1302-1310 (2011).
 21. T. W. Berg and J. Mork, "Saturation and noise properties of quantum-dot optical amplifiers," *IEEE J. Quantum Electron.* **40**, 1527-1539 (2004).
 22. Y. Ding, M. A. Cataluna, D. Nikitichev, I. Krestnikov, D. Livshits, and E. Rafailov, "Broad Repetition-Rate Tunable Quantum-Dot External-Cavity Passively Mode-Locked Laser with Extremely Narrow Radio Frequency Linewidth," *Appl. Phys. Express* **4**, 062703 (2011).
 23. Y. Ding, D. I. Nikitichev, I. Krestnikov, D. Livshits, M. A. Cataluna, and E. U. Rafailov, "Fundamental and harmonic mode-locking with pulse repetition rate between 200 MHz and 6.8 GHz in a quantum-dot external-cavity laser," in *Lasers and Electro-Optics Europe (CLEO EUROPE/EQEC), 2011 Conference on and 12th European Quantum Electronics Conference*, (Munich, Germany, 2011), p. CF_P23.
 24. M. Xia, M. G. Thompson, R. V. Penty, and I. H. White, "External-Cavity Mode-Locked Quantum-Dot Laser Diodes for Low Repetition Rate, Sub-Picosecond Pulse Generation," *IEEE J. Sel. Top. Quantum Electron.* **17**, 1264-1271 (2011).
 25. Y. Ding, D. I. Nikitichev, I. Krestnikov, D. Livshits, M. A. Cataluna, and E. U. Rafailov, "Quantum-dot external-cavity passively modelocked laser with high peak power and pulse energy," *Electron. Lett.* **46**, 1516-1517 (2010).
 26. R. Koda, T. Oki, T. Miyajima, H. Watanabe, M. Kuramoto, M. Ikeda, and H. Yokoyama, "100 W peak-power 1 GHz repetition picoseconds optical pulse generation using blue-violet GaInN diode laser mode-locked oscillator and optical amplifier," *Appl. Phys. Lett.* **97**, 021101 (2010).
 27. M. Drobizhev, N. S. Makarov, S. E. Tillo, T. E. Hughes, and A. Rebane, "Two-photon absorption properties of fluorescent proteins," *Nat. Methods* **8**, 393-399 (2011).
-

1. Introduction

High peak-power ultrafast laser systems are key elements in a number of biomedical imaging applications. This is the case for nonlinear microscopy (NLM), where excitation occurs only when two (or more) photons coincide in space and time. Therefore, a high photon flux density (in space and time) is required. The first condition can be achieved through the use of a high numerical aperture microscope objective and the second by employing ultrashort pulsed lasers. The combination of these two conditions produces the required peak intensities for generating a nonlinear effect (while maintaining average powers at a suitable level compatible with biological samples). These conditions also ensure that any generated light is only produced within the optical section to be imaged [1]. Currently, most NLMs employ the classic ultrashort pulsed Ti:Sapphire laser source, extensively used in research laboratories as it combines a broad tunability range, together with the required output peak powers to generate nonlinear images [2-3]. However, such lasers are bulky, expensive and normally require mechanical isolation tables. Furthermore, such laser systems include a high-power

pump laser and are normally composed of several elements which make the whole system difficult to operate. They require, therefore, continuous maintenance (including realignment and cleaning) or need to rely on expensive vacuum-sealed computer-controlled enclosing boxes to achieve efficient operation. In principle, an ideal excitation source for nonlinear imaging should be able to excite several fluorophores, be cost-effective, easy to use, reliable and compact. If these conditions are met, such excitation sources could potentially replace the expensive and bulky solid-state ultrafast laser sources. In order to be able to make relative comparisons between the applicability of laser sources for NLM applications, a figure-of-merit (FOM) can be defined as a function of their average power, pulse duration, and repetition rate [4]. The FOM is defined as the product of the average power and the peak power ($P_{avg} \times P_{peak}$), which can be recast into the equation: $P_{avg}^2 / (f_{rep} \cdot \Delta\tau)$, where f_{rep} and $\Delta\tau$ are the repetition rate and the pulse duration, respectively. Moreover, this value is useful for determining if the laser source is suitable for nonlinear excitation as the detected signal level from a two-photon process is proportional to this FOM [5].

Ultrafast lasers within the wavelength range of ~700 nm to 1000 nm, particularly at wavelengths near 800 nm (where the Ti:Sapphire lasers operate most efficiently), have been used as excitation sources for two-photon excited fluorescence imaging (TPEF) [6] and other nonlinear imaging techniques such as those using second harmonic generation [7-8]. In the past years, a few semiconductor laser diode systems with amplification schemes have been successfully demonstrated as light sources for NLM applications at the abovementioned waveband [9-11]. These laser diode systems typically involved two or more stages of amplification (based on semiconductor and/or fiber amplifiers), as well as extra-cavity dispersion compensation schemes. Very recently, NLM imaging has been demonstrated with a compact, picosecond, vertical external-cavity surface-emitting laser emitting at 965 nm [4]. This device was able to efficiently produce TPEF images of several fluorescent markers including green fluorescent protein, as the laser's emission wavelength virtually matched the maximum two-photon action cross section of this protein.

In addition to the above, ultrafast lasers operating at longer wavelengths are of great interest for deep tissue imaging. Indeed, high contrast imaging of different tissues at approximately twice the depth has been demonstrated with 1280-nm excitation, when compared to 775-nm excitation (generated by a Ti:Sapphire-pumped optical parametric oscillator and a Ti:Sapphire laser, respectively) [12]. The advantages of this spectral band for NLM applications are therefore linked to the larger penetration depths which result from decreased scattering [12], and the reduced probability of photo-damage [13]. As a result, the use of ultrafast lasers emitting within the ~1.2-1.3 μm spectral range is showing a great promise for commercial NLM applications. In this context, compact Cr:Forsterite lasers emitting at 1230 nm have been demonstrated as excitation sources for NLM with great success [14-15].

In this paper, we present the first semiconductor pulsed laser diode system within the spectral range between 1.0 μm and 1.3 μm with characteristics which are compatible with NLM applications. The laser system here demonstrated is a master-oscillator power-amplifier (MOPA) based on a QD-ECMLL, amplified by a tapered QD-SOA, with emission in the 1.26 μm spectral band. Both devices were based on InAs/GaAs QD structures, as these materials can be routinely grown to cover the spectral range between 1.0 μm and 1.3 μm , in addition to offering important advantages in the context of ultrashort-pulsed lasers such as ultrafast carrier dynamics, broad gain/absorption bandwidth, excellent noise characteristics and low optical losses [16-20]. Moreover, QD-based SOAs are extremely suitable for boosting the power of ultrashort pulses due to their high gain saturation characteristics, broad gain bandwidth, fast gain recovery times and low noise figure exhibited by these devices [21]. The choice of an external-cavity mode-locking configuration in this work is associated with the possibility to access lower repetition rates than what are typically achievable with

monolithic lasers, as well as offering the possibility to easily vary the pulse repetition rate [20, 22-24].

In our previous work, we demonstrated the generation of high-peak-power picosecond pulses with pulse repetition rate from 2.4 GHz to 1.14 GHz [25] and from 1 GHz to 191 MHz [22] from a single QD-ECMLL, using 96% and 53% output couplers as the external cavity facets, respectively. For a pulse repetition rate of 1.14 GHz, an average power of 23.2 mW and a peak power of 1.5 W with pulse duration of 13.6 ps were achieved, which corresponds to a 20.4-pJ pulse energy [25].

In this paper, we present a new external-cavity design which used a chirped volume Bragg grating as an external cavity output coupler. The output power from the pulsed oscillator was boosted by a tapered QD-SOA with a similar epitaxial structure in order to maximize mode matching between the oscillator and amplifier. Taking advantage of the versatility offered by the external-cavity oscillator, the performance of the MOPA system was characterized for two different pulse repetition rates. By keeping the pulse energy or peak power of the amplifier input constant, it has been verified that a lower repetition rate corresponding to a lower average input power resulted in a higher SOA gain and a higher peak power, due to the gain saturation characteristics of the SOA. As a result, for a pulse repetition rate of 1.1 GHz, an average power of 294 mW, pulse energy of 267 pJ, peak power of 26.3 W and FOM of 7.73 W^2 were achieved. With a lower repetition rate of 648 MHz, a higher peak power of 30.3 W was achieved together with a 208.2 mW average power, 321 pJ pulse energy and 6.31 W^2 FOM. To the best of our knowledge, these values represent the best results ever to be demonstrated for the high peak-power picosecond optical pulse generation from an all-semiconductor laser diode system in the spectral region between $1.0 \mu\text{m}$ and $1.3 \mu\text{m}$. Moreover, we present preliminary results of the first demonstration of NLM using a laser diode-based system with a single amplification stage and without external pulse compression, which represents a step change from previous NLM results achieved with diode-based systems [9-11].

2. Experimental setup

The schematic of the experimental setup is shown in Fig. 1. The QD-MOPA system consists of a QD-ECMLL based on a two-section gain chip or superluminescent diode (SLD) and a chirped volume Bragg grating (CBG) used as an external cavity output coupler together with a tilted and tapered QD-SOA for amplifying the pulse power from QD-ECMLL.

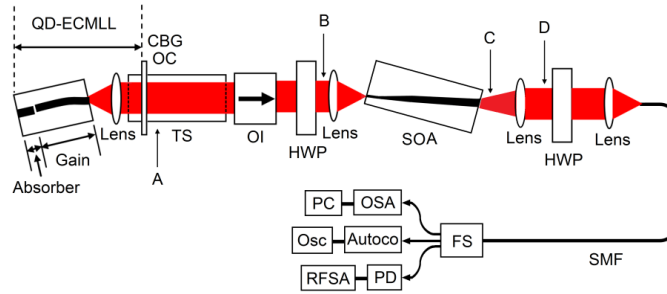


Fig. 1. Configuration of a QD-MOPA system and the experimental setup. CBG OC: chirped Bragg grating output coupler; TS: motorized translation stage; OI: optical isolator; HWP: half wave plate; SOA: semiconductor optical amplifier; SMF: single-mode fiber; FS: fiber splitter; OSA: optical spectrum analyzer; PC: Personal computer; Autoco: autocorrelator; Osc: oscilloscope; PD: photo detector; RFSA: RF spectrum analyzer.

Both the SLD and tapered SOA were fabricated from wafers with similar epitaxial structure grown on an n^+ -GaAs (100) substrate by molecular beam epitaxy which contained 10 layers of self-assembled InAs/GaAs quantum dots. The wavelength and optical mode matching between QD lasers and QD amplifiers were important factors in the decision to adopt identical QD structures as active regions of both devices in this work. Both wafers were grown by Innolume, but not in the same epitaxial batch. The two-section gain chip was fabricated by Innolume, whereas the tapered SOA was fabricated by III-V Lab according to the design and simulations carried out by the teams at the Politecnico di Torino and the National and Kapodistrian University of Athens (further details on the simulation and design of this and other tapered QD-SOAs will be published elsewhere).

The two-section SLD chip used for the QD-ECMLL consisted of a gain section and a saturable absorber section. The waveguide in the gain section was bent and terminated at an angle of 7° relative to the cleaved facet with an antireflection (AR) coating ($R \sim 10^{-5}$); the back facet was high-reflection coated ($R \sim 95\%$). The total chip length was 4 mm, with an 800 μm -long saturable absorber section (20% absorber-to-total-length ratio) placed near the back facet.

As mentioned above, the output coupler employed was a CBG, sourced from Optigrate Corp. The CBG is a reflective Bragg grating inscribed in photo-thermal-refractive glass. The chirp is made possible through the grating period variation in the direction of beam propagation, which imparts different delays to different spectral components reflected along the CBG. In this work we used a CBG with an optical aperture of 5 mm x 6 mm, a thickness of 2 mm and a center wavelength of about 1262 nm. The CBG's reflectivity (or diffraction efficiency) was around $\sim 12\text{-}15\%$. The CBG was mounted on a motorized translation stage in order to obtain an accurate tunability of the pulse repetition rate.

A collimating aspherical lens with a numerical aperture of 0.55 was used to couple light to and from the SLD chip. The output beam from the seed laser source was coupled onto the input facet of SOA after optical isolation and polarization control.

The total length of the SOA chip was 6 mm. The waveguide width changed from 14 μm at the input facet to 80 μm at the output facet. Both the input and output facets of the SOAs were AR-coated, which in combination with a tilted waveguide resulted in a residual reflectivity of $\sim 10^{-5}$.

The output beam from the SOA was collimated and focused onto a single-mode fibre-splitter and coupled to an autocorrelator, a radio-frequency (RF) spectrum analyzer and an optical spectrum analyzer (OSA) for characterization of the MOPA output. Using a mirror flipper inserted between the oscillator and amplifier, the pulsed output from the QD-ECMLL was also characterized, in order to compare the pulse characteristics of the input pulses to the SOA and resulting amplified pulses. Both the SLD and SOA chips were mounted on AlN submounts and copper heatsinks, and were kept at 20°C using a thermoelectric temperature controller during the experimental work.

3. Experimental results and discussion

3.1 Continuous-wave operation of the MOPA system

The continuous-wave (CW) operation of the MOPA system was characterized prior to the investigation of the MOPA's performance under pulsed operation.

In order to achieve CW operation, a forward bias was applied to the gain section of the two-section SLD in the QD-ECMLL, while the saturable absorber section was left unbiased. The CW amplified power (red) from the SOA and its gain (black) as a function of the current applied to the SOA are represented in Fig. 2. The output power represented is the power obtained from the SOA, after subtracting the power contribution from the broadband amplified spontaneous emission generated by the SOA (which was measured without the

oscillator input). For example, under an injection current of 3120 mA applied to the SOA, the measured output power from the SOA and the ASE power were 676 mW and 224 mW, respectively – resulting in an output power of 452 mW, as represented in Fig. 2. The gain of the SOA presented here is the ratio of the output power (the power after collimation from the SOA output facet, measured at point D in Fig. 1, subtracted of all the ASE power) to the input power (the power before coupling towards the SOA input facet, measured at point B in Fig. 1). The real SOA chip gain is unknown because the input coupling efficiency cannot be accurately determined. It is important to note that in this graph and throughout the paper, only the “worst-case” scenario is represented, as we have subtracted all the ASE contributions from the output powers and corresponding gains. We have therefore assumed that no ASE power is converted into the oscillator input (whether under CW or pulsed operation), in order to simplify the analysis and avoid a possible overestimation of the output power, as there is a degree of uncertainty in the quantification of the amount of “useful” ASE that is coupled to the SOA input (whether pulsed or CW), and thus only a range of such coupled ASE power can be estimated, rather than an actual value – this is illustrated in the recent paper by Koda *et al.* [26].

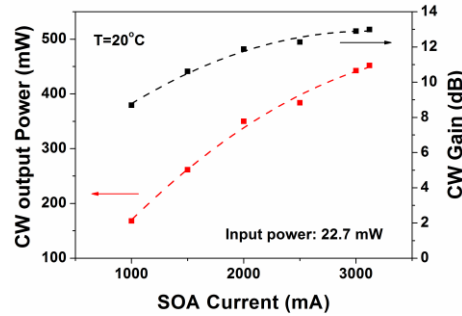


Fig. 2. CW output power (red) and gain (black) versus SOA current at 20 °C.

The 3-dB saturation output power of the SOA chip for CW input is about 316 mW (~25 dBm) under 2000-mA injection current. Beyond the 3-dB saturation output power point, the gain dropped quickly with increasing input power. Knowing the 3-dB saturation output power of the SOA, one can estimate the possible maximum pulse peak power produced by the MOPA system under pulsed operation, considering the inverse of the duty cycle associated with both a particular pulse duration and pulse repetition frequency (and assuming that the amplification for the pulsed and CW regimes is not distinct). A gradually saturated output power can be observed with an increasing SOA current, especially close to 3000 mA, when the input CW power is 22.7 mW (13.5 dBm). From the trend of the gain increase with increasing SOA current in Fig. 2, we know that a higher power can be obtained under a higher SOA current, but accompanied with the risk of thermal saturation problems and pulse broadening for the pulsed input.

Finally, it should also be noted that the output power from the SOA measured with an integrating sphere photodiode power sensor at point C was 1.17-1.25 times higher than with a conventional (non-integrating-sphere type) detector at point D, which is caused by the collimating lens loss. We estimated the lens efficiency to be a maximum of 85% and used this value to estimate the actual power generated by SOA according to the measured value from the conventional detector [26]. As such, the actual maximum CW output power is estimated to be 532 mW (452mW/0.85), under the bias conditions investigated in this work.

3.2 Picosecond operation of the MOPA system

We investigated the performance of the MOPA system under pulsed operation for two different pulse repetition rates of the QD-ECMLL oscillator: 1.1 GHz and 648 MHz.

The light-current ($L-I$) characteristics of the QD-ECMLL oscillator for both repetition rates are shown in Fig. 3 (measured at point A of Fig. 1). For a 0 V reverse bias applied to the saturable absorber section of the two-section SLD, the oscillator is under CW operation and both $L-I$ curves are almost overlapped. On the other hand, for a 4 V reverse bias applied to the saturable absorber, the ratio of output power for both repetition rates is almost proportional to the ratio of the corresponding repetition rates, which is consistent with our previous investigation, whereby the two-section SLD had a 15% absorber-to-total-length-ratio and the output coupler was a conventional one [20]. It should be noted that mode-locked operation can be attained for much lower values of forward current and reverse bias than in the previous work, owing to the use of a 20% absorber-to-total-length-ratio and a CBG output coupler.

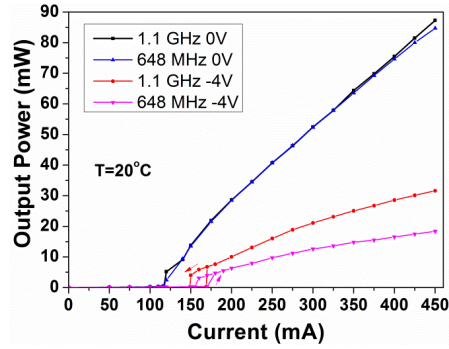


Fig. 3. $L-I$ characteristics of QD-ECMLL with 20% SA to length ratio and CBG external cavity output coupler for 0 and 4-V reverse bias at 1.1 GHz and 648 MHz repetition rates.

Under mode-locked operation at a pulse repetition rate of 1.1 GHz, the pulsed output of the QD-ECMLL was characterized (without amplification). In Fig. 4, the autocorrelation trace, optical spectrum, RF spectrum with both 200-MHz span and 20-GHz span are represented, for the case of a reverse bias of 4 V and forward current of 200 mA applied to the two-section SLD. The autocorrelation was fitted by a Lorentzian function, as it provided the best fit among conventional fitting functions. Moreover, the corresponding optical spectrum was also well fitted by a Lorentzian function (this was also the case for all the autocorrelation traces and optical spectra represented in this paper). An average power of ~ 10 mW was measured at the position after the optical isolator and half-wave plate (point B in Fig. 1). 1 W peak power and about 9-ps pulses were generated directly from the QD-ECMLL.

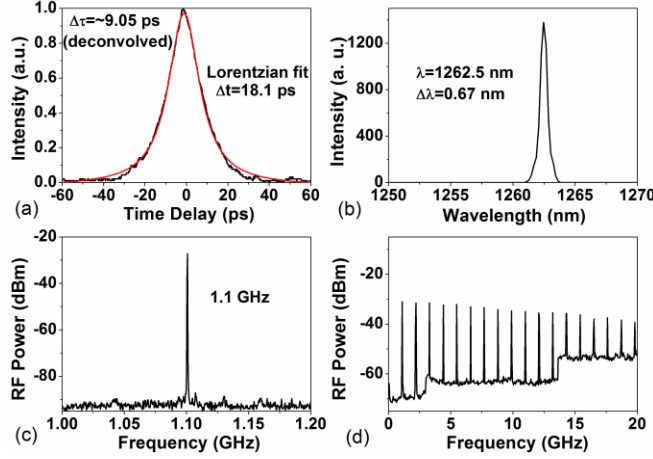


Fig. 4. (a) Autocorrelation trace, (b) optical spectrum, (c) RF spectrum with 200-MHz span, and (d) RF spectrum with 20-GHz span, at reverse bias of 4 V and forward current of 200 mA with a pulse repetition rate of 1.1 GHz directly from the QD-ECMLL at 20 °C.

While keeping the same bias conditions applied to the QD-ECMLL gain chip, the MOPA output was characterized as a function of the current applied to the QD-SOA, ranging from 1000 mA to 3000 mA (pulse repetition rate of 1.1 GHz). The autocorrelation trace, optical spectrum and RF spectra are shown in Fig. 5, for a 3000-mA current applied to the SOA. Comparing the results represented in Fig. 4(a) with Fig. 5(a), we can find that the pulse broadening after 3000-mA SOA amplification is about 12.5%. The RF signal exhibits a high dynamic contrast and a large number of harmonics in Fig. 5(d), indicating that the high quality of mode-locking was kept after amplification. Some residual ASE contribution can still be seen in the optical spectrum in Fig. 5(b), due to a strong ASE at a high current, despite the fact that a bandpass filter was used here (filter with a central wavelength of 1262 nm and a bandwidth of 10 nm).

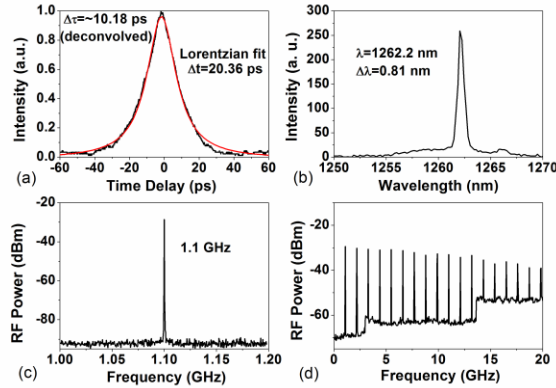


Fig. 5. (a) Autocorrelation trace, (b) optical spectrum, (b) RF spectrum with 200-MHz span, and (d) RF spectrum with 20-GHz span, for a pulsed input at a pulse repetition rate of 1.1 GHz and a current of 3000 mA applied to the SOA at 20 °C.

For the same repetition rate (1.1 GHz), we subsequently investigated the dependence of the peak power, gain, average power, and FOM on SOA current after collimation (point D in

Fig. 1). The results are represented in Fig. 6. Using the same approach as detailed in section 3.1, we assumed the worst-case scenario for the representation of the output power and subtracted all the ASE power (measured without input) to the output power (this approach is followed throughout the paper).

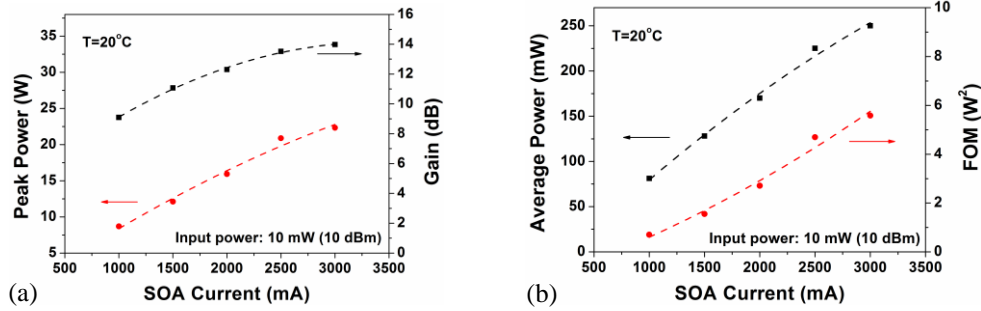


Fig. 6. Peak power (red), gain (black), average power (black), and FOM (red) against SOA current for a 1.1-GHz repetition rate.

Note that, as in section 3.1, the measured (and represented) output power should be further multiplied by an inverse factor of 0.85 to correct for the 85% collimating lens efficiency in order to estimate the amplified pulse power generated directly by the SOA. As shown in Fig. 6 (a), the highest peak power of 22.35 W divided by 0.85 resulted in a peak power of 26.3 W. Likewise, a corrected average power of 294 mW (250/0.85 mW) (267 pJ pulse energy) and FOM of 7.73 W² (5.59/(0.85×0.85) W²) can be obtained at the highest SOA current of 3000 mA.

In order to investigate the amplification performance with a lower pulse repetition rate, we extended the cavity length of the QD-ECMLL, thus changing its pulse repetition rate from 1.1 GHz (10 mW power, see Fig. 3 red line) to 648 MHz (6 mW power, see Fig.3 magenta line), while keeping the same bias conditions applied to the two-section SLD (reverse bias of 4 V and forward current of 200 mA). The autocorrelation trace, optical spectrum and RF spectra measured directly from the QD-ECMLL at a pulse repetition rate of 648 MHz are shown in Fig. 7. An average power of ~6 mW was measured at point B in Fig. 1. Similarly with the case at 1.1 GHz repetition rate, a peak power of around 1 W and about a 9 ps pulse can be achieved from the QD-ECMLL, because the constant pulse energy required to saturate the absorber is independent of the repetition rate under certain operation conditions, which is consistent the conclusions reported in Ref. 20. The wavelength for both repetition rates is around 1262.3-1262.5 nm which is determined by the CBG central wavelength.

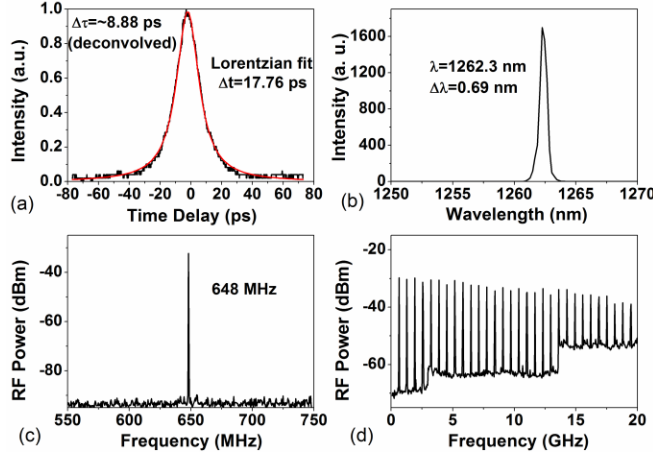


Fig. 7. (a) Autocorrelation trace, (b) optical spectrum, (c) RF spectrum with 200-MHz span, and (d) RF spectrum with 20-GHz span, at reverse bias of 4 V and forward current of 200 mA with a pulse repetition rate of 648 MHz for the QD-ECMLL without amplification at 20 °C.

The QD-ECMLL's pulsed output (as illustrated in Fig. 7) was then used as an input to the tapered QD-SOA. Fig. 8 exhibits the autocorrelation trace, optical spectrum and RF spectra of the amplified pulsed output at 648 MHz, for a 2500 mA current applied to the SOA. The measured RF signal displays a high dynamic contrast and a large number of harmonics in Fig. 8(d), indicating that the quality of mode-locking is preserved after amplification, similar to the performance previously obtained for the MOPA configuration with 1.1-GHz pulse repetition rate.

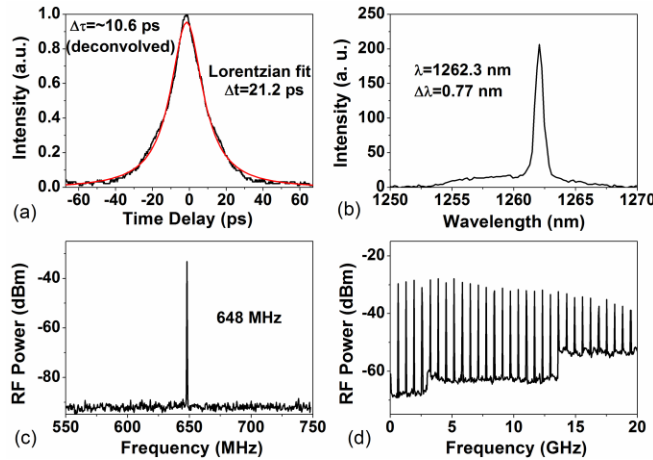


Fig. 8. (a) Autocorrelation trace, (b) optical spectrum, (c) RF spectrum with 200-MHz span, and (d) RF spectrum with 20-GHz span, for a pulse repetition rate of 648 MHz and SOA current of 2500 mA at 20 °C.

The dependence of the peak power, gain, average power, and FOM for the 648 MHz repetition rate was then investigated as a function of the current applied to the SOA (from 1000 mA to 2500 mA), as depicted in Fig. 9.

The average power as represented in Fig. 9 was measured at point D in Fig. 1 – after collimation. Therefore, the same technique can be applied as previously to account for the collimation lens losses (15%) and we estimate that the highest peak power of 30.3 W can be achieved directly from the SOA under these conditions (25.8 W/0.85). Likewise, a corrected average power of 208 mW (177/0.85 mW) and FOM of 6.3 W² (4.56/(0.85×0.85) W²) can be obtained at the highest SOA current of 2500 mA (Fig. 9 (b)). The corresponding pulse energy is 321 pJ, which represents a ~13-fold increase when compared to the current state-of-the-art for semiconductor lasers at the 1.26 μm waveband [25].

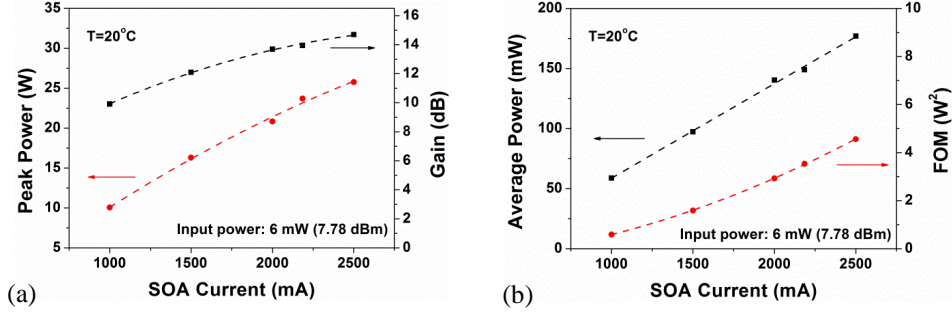


Fig. 9. (a) Peak power (red), gain (black), (b) average power (black), and FOM (red) against SOA current for a 648-MHz repetition rate.

3.3 Discussion of the results

Before discussing the amplification results, we would like to comment on the performance obtained with the QD-ECMLL oscillator. The 20% absorber-to-length ratio used in this work required a lower reverse bias compared to the 15% absorber-to-length ratio structure which we used in our previous study [22, 25], and the pulse was slightly narrower under similar operation conditions. In this work, we also demonstrated the use of a CBG as an external-cavity output coupler, for the first time. The original intention for adopting a CBG as an output coupler was to lock the spectral emission bandwidth and compress the pulse through intracavity dispersion compensation. However, we did not observe the anticipated effects of pulse narrowing with the CBG output coupler when compared to a generic output coupler with similar (broadband) reflectivity. This observation could be due to the insufficient effective grating length, which therefore did not provide enough dispersion compensation for the chirped pulses. Nevertheless, we found the mode-locking regime obtained with the CBG output coupler was more stable than with a broadband output coupler, and the lasing wavelength was exactly fixed at the CBG wavelength - unlike the mode-locking behavior obtained from a QD-ECMLL with a conventional output coupler, where a wander of central emission wavelength can occur, depending on the interplay of the reverse bias and injection current. The significance of this finding is that QD-ECMLLs can be implemented with very stable spectral characteristics, independently of the various mode-locking operation conditions and operating temperature.

For demonstrating the results presented in this paper, we harnessed the advantage of using a QD-ECMLL as an oscillator, enabling the delivery of a low-repetition-rate pulsed output, which resulted in a low duty cycle and a relatively low average power, when compared to the monolithic mode-locked lasers. This approach allowed us to boost the achievable gain from the tapered QD-SOA, thus enabling the generation of high-peak power pulses from the MOPA system.

Regarding the overall performance of the MOPA system, a comparison of the amplification results obtained for the 1.1 GHz and 648 MHz pulsed output with the same peak power highlights that the SOA gain was enhanced, as expected, from 12.3 dB for 1.1 GHz repetition rate to 13.7 dB for 648 MHz (under the same applied SOA current of 2000 mA, corresponding to a SOA current density of ~ 600 A/cm²). Indeed, the corresponding input average power was 10 mW (10 dBm) for the 1.1 GHz case, as opposed to 6 mW (7.78 dBm) for the 648 MHz repetition rate. Therefore, even though the peak power and pulse energy at the SOA input can be kept constant under different repetition rates, a higher peak power as well as a higher pulse energy can be achieved from the SOA output for a lower repetition rate. However, the average power and FOM after amplification became lower for a decreased repetition rate.

Some aspects of the current demonstration could be improved in future work, in order to further boost the achievable peak power. One of these aspects is related to spectral mismatch. This is illustrated in the discrepancy between the spectral characteristics of the QD-ECMLL, with an emission wavelength centred at about 1262 nm (dictated by the CBG), and the tapered SOA, which displays an ASE spectrum centred at 1251.4 nm, with a 3-dB bandwidth of 17 nm (at 1200 mA). Despite the fact that two identical epitaxial structures were chosen for the two-section SLD and tapered QD-SOA, there was a mismatch of nearly 15 nm between the central emission wavelength (the free-running SLD emission was centred around 1266 nm). Due to the difference between the SOA center wavelength and external cavity lasing wavelength (1262 nm) in this work, detuning between the SOA gain and input laser might have contributed to a sub-optimal gain in the SOA. In the future, a closer spectral matching in the MOPA system will be helpful to further improve the output power from the SOA. This can be achieved by shifting either the laser or the SOA wavelength, through changing the device's operation temperature, using a more suitable CBG or including a flexible means to select the oscillator's emission wavelength. Ultimately, both devices could be fabricated from the same wafer to ensure such spectral match. The coupling efficiency between the oscillator and amplifier could also be the subject of improvement.

Additionally, it is also possible to lower the repetition rate of this QD-ECMLL further [22]. With the insights gained from this work, it is foreseeable that lower repetition rates will lead to even higher values of peak power.

We predict that the achievable gain in the tapered QD-SOA could also be increased with the use of a different epitaxial structure which could incorporate QD layers with more uniform QD sizes in its active region, leading to higher values of modal gain at the input laser wavelength. The optical confinement factor could also be reduced to increase the saturation energy. Furthermore, pulse compression schemes could be implemented by using either an intra-cavity etalon in the QD-ECMLL, as successfully demonstrated in [24], or an external dispersion compensation setup after the tapered QD-SOA.

3.4 Nonlinear imaging application of the picosecond MOPA system

The QD-MOPA prototype was installed and tested as an ultrashort pulsed light source for nonlinear imaging applications. The collimated SOA output was air-coupled to an inverted microscope (Nikon, Eclipse TE 2000U). The beam was expanded to fill the back aperture of a CFI Apochromatic, oil immersion, 60x microscope objective with a numerical aperture of 1.4 (λ S, Nikon). The sample was scanned in the x-y directions using a translation stage (Tango, Märzhäuser Wetzlar). To acquire the TPEF image, a band pass filter (KG3, Schott) was placed in front of a photomultiplier tube (Hamamatsu, H9305-03), as shown in Fig. 10. The two-section SLD was operated under a reverse bias of 4 V and a forward current of 200 mA, with the QD-ECMLL generating optical pulses at a repetition rate of 648 MHz. The tapered SOA current was 2000 mA. Both semiconductor devices operated at 20°C.

For the nonlinear imaging demonstration, 15- μm crimson fluorescent microspheres (Invitrogen, F-8839) were used. These were placed in water solution, sandwiched between two cover glasses. This sample can be excited using $\sim 625\text{ nm}$ if a linear excitation scheme is considered; however, in our case the two-photon action cross-section of Crimson dye at 1260 nm is $\sim 16\text{ GM}$ [27] - under this condition a few Watts of peak power together with the laser repetition rate would enable the production of nonlinear images of such a sample [4]. The available peak power at the sample plane was $\sim 3\text{-}4\text{ W}$ at the operating wavelength (1.26 μm) of the MOPA system (the microscope objective measured transmission was $\sim 28\%$). Despite the low peak powers, the imaged sample could be observed as shown in Fig. 10. To the best of our knowledge this is the first demonstration of TPEF imaging obtained with a semiconductor-based ultrafast laser system within the spectral range of 1.0 μm - 1.3 μm .

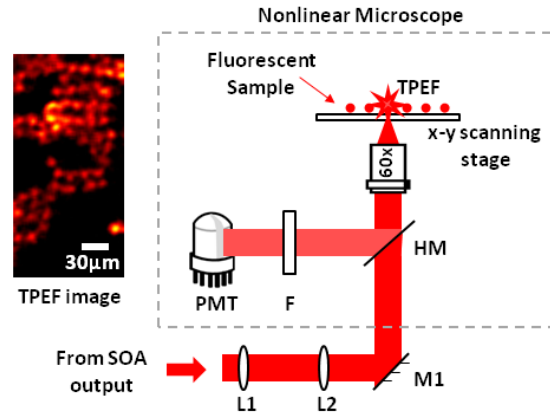


Fig. 10 The left panel is the TPEF image of 15 μm Crimson fluorescent beads obtained at ICFO with the QD-MOPA system. The resulting image was obtained by averaging 10 frames to improve the signal to noise ratio. The right panel is a simplified schematic of the nonlinear microscope setup. L#: lenses; M#: mirror; HM: dichroic mirror; F: bandpass filter; PMT: photomultiplier tube.

Although this system operates at a fixed wavelength, it could also be used to efficiently excite a wide range of fluorescent dyes via TPEF, such as: the mKate variants; TurboFP635; TurboFP650; mRaspberry; mPlum; mGrape3; Neptune; NirFP; mNeptune; etc, as these have similar or higher two-photon action cross-sections compared to the Crimson dye [27].

In the present work, an ultrashort pulsed laser system based on chip-scale devices, having modest power requirements, and based on QDs, has been developed. Its output peak power characteristics have enabled TPEF imaging as a proof-of-concept demonstration.

Future improvements will have to be carried out to increase the peak power from the SOA output, as described in the previous section. Moreover, the improvement of the coupling efficiency of the laser towards the NLM will be explored.

4. Conclusion

The ultrashort-pulsed MOPA system presented in this paper is the first demonstration of a low-cost, chip-scale based device in the spectral region 1.0 μm - 1.3 μm , with power levels compatible with NLM. The system generates high-peak power picosecond optical pulses centered at 1.26 μm , which is located within the infrared penetration window of most biological tissues. This asset could potentially offer greater penetration depths and reduced sample damage compared with the ultrashort-pulsed semiconductor laser systems previously

demonstrated, which could lead to major progress and a more widespread adoption of nonlinear imaging technology. Moreover, and unlike previous demonstrations of nonlinear imaging with ultrafast laser diode systems, we present for the first time a system which incorporates only a single amplification stage, and does not include external dispersion compensation, enabling a rather more compact and less complex laser system.

For a pulse repetition rate of 1.1 GHz, an average power of 294 mW, a pulse energy of 267 pJ, a peak power of 26.3 W and FOM of 7.73 W² were achieved from the QD-MOPA system. Importantly, by lowering the repetition rate to 648 MHz, a higher peak power of 30.3 W was achieved together with a 208.2-mW average power, a 321-pJ pulse energy and a 6.31 W² FOM. Using a constant pulse energy and peak power as the input, we have demonstrated that a lower repetition rate - corresponding to a lower average input power - enabled a higher SOA gain and consequently the generation of higher peak power (and energy) pulses, due to the gain saturation characteristics of the SOA.

Preliminary TPEF imaging results indicate that this QD laser system is promising as a high peak-power pulsed light source, with a wavelength emission that could potentially cover 1.0 μm - 1.3 μm, which is very useful for nonlinear bio-imaging applications.

Acknowledgements The work was funded within the Seventh Framework Program “FAST-DOT”, through Grant No. 224338. M. A. Cataluna acknowledges also financial support through a Royal Academy of Engineering/EPSRC Research Fellowship. Y. Ding acknowledges financial support from a Marie Curie Fellowship. This work is supported by the Generalitat de Catalunya grant 2009-SGR-159, the Spanish government grant TEC2009-09698, the NoE P4L, and Laserlab optobio. We thank Nikon instruments Spain for providing the microscope objective used in this work. This research has been partially supported by Fundació Cellex Barcelona and has been partially conducted at ICFO’s “Super-Resolution Light Microscopy and Nanoscopy Facility” (SLN@ICFO).